Applied Radiation and Isotopes 208 (2024) 111275

Contents lists available at ScienceDirect

Applied Radiation and Isotopes

journal homepage: www.elsevier.com/locate/apradiso

Methodology for measuring photonuclear reaction cross sections with an electron accelerator based on Bayesian analysis

Saverio Braccini [a], Pierluigi Casolaro [a,e,f], Gaia Dellepiane [a], Christian Kottler [b], Matthias Lüthi [b,d,*], Lorenzo Mercolli [a,c], Peter Peier [b], Paola Scampoli [a,e], Andreas Türler [d]

[a] Albert Einstein Center for Fundamental Physics (AEC), Laboratory for High Energy Physics (LHEP), University of Bern, 3012, Bern, Switzerland
[b] Federal Institute of Metrology METAS, 3003, Bern-Wabern, Switzerland
[c] Department of Nuclear Medicine, Inselspital, Bern University Hospital, University of Bern, 3010, Bern, Switzerland
[d] Department of Chemistry, Biochemistry, and Pharmaceutical Sciences (DCBP), University of Bern, 3012, Bern, Switzerland
[e] Department of Physics "Ettore Pancini", University of Napoli Federico II, Complesso Universitario di Monte S. Angelo, 80126, Napoli, Italy
[f] INFN Naples Unit, Naples, Italy

ARTICLE INFO

Dataset link: https://doi.org/10.5281/zenodo.10790863

Keywords:
Photonuclear reactions
Cross section
Bayesian analysis
Electron accelerator

ABSTRACT

Accurate measurements of photonuclear reaction cross sections are crucial for a number of applications, including radiation shielding design, absorbed dose calculations, reactor physics and engineering, nuclear safeguard and inspection, astrophysics, and nuclear medicine. Primarily motivated by the study of the production of selected radionuclides with high-energy photon beams (mainly ^{225}Ac, ^{47}Sc, and ^{67}Cu), we have established a methodology for the measurement of photonuclear reaction cross sections with the microtron accelerator available at the Swiss Federal Institute of Metrology (METAS). The proposed methodology is based on the measurement of the produced activity with a High Purity Germanium (HPGe) spectrometer and on the knowledge of the photon fluence spectrum through Monte Carlo simulations. The data analysis is performed by applying a Bayesian fitting procedure to the experimental data and by assuming a functional trend of the cross section, in our case a Breit-Wigner function. We validated the entire methodology by measuring a well-established photonuclear cross section, namely the ^{197}Au(γ, n)^{196}Au reaction. The results are consistent with those reported in the literature.

1. Introduction

Photonuclear reactions occur when megaelectronvolt photons undergo inelastic interaction with a nucleus. At photon energies below 25 MeV to 30 MeV, the excitation function of photonuclear reactions is characterized by a prominent peak, known as giant dipole resonance (GDR). This is a collective excitation of the atomic nucleus wherein nucleons move together, creating a large oscillation of the nucleus in the shape of a dipole. This energy range matches the upper limit of most electron accelerators, which produce X-rays by "Bremsstrahlung". This process involves slowing down (or stopping completely, depending on the thickness of the target) the electrons in a target. The photon flux scales approximately quadratically with the target atomic number, thus high Z materials are typically selected as converter targets. The most commonly used are gold, tantalum or tungsten, although the use of lighter materials such as niobium and copper is also reported (Zilges et al., 2022). Experimentally, measuring photonuclear cross-sections at bremsstrahlung facilities is challenging. The reaction yield is a convolution of the cross-section and of the continuous X-ray energy spectrum, and the yield curve can be experimentally determined by varying the electron energy. Consequently, the cross-section information is extracted by unfolding methods. This relies heavily on the knowledge of the energy spectrum (which is difficult to measure), reproducibility of the accelerator output, and high counting statistics. To circumvent the issues of a bremsstrahlung spectrum, the production of high-energy X-rays has also been achieved using other techniques, including Laser-Compton Scattering (LCS). While bremsstrahlung generally produces a larger number of photons, LCS has the advantage of producing quasi-monochromatic gamma rays, which allow avoiding the use of unfolding methods (Turturica et al., 2019). Despite these challenges, there is now a substantial amount of measured data available from photonuclear reactions. In this context, the International Atomic Energy Agency (IAEA) issued a comprehensive review on photonuclear data, emphasizing the importance of the accurate knowledge of photonuclear reaction cross-sections for several applications (Kawano et al., 2020), including radiation shielding design and transport analyses, calculation

* Corresponding author.
E-mail addresses: pierluigi.casolaro@unina.it (P. Casolaro), matthias.luethi@metas.ch (M. Lüthi).

https://doi.org/10.1016/j.apradiso.2024.111275
Received 15 September 2023; Received in revised form 9 February 2024; Accepted 1 March 2024
Available online 2 March 2024

of the absorbed dose in human body for radiotherapy, physics, and technology of fission and fusion reactors, activation analyses, safeguards and inspection technologies, nuclear waste transmutation, and astrophysical nucleosynthesis.

In the last decade, the possibility of using photonuclear reactions for the production of radionuclides for nuclear medicine has been established (Maslov et al., 2006; Rane et al., 2015; Mamtimin et al., 2015; Starovoitova et al., 2014). The renewed interest in this topic was sparked by the commercial availability of compact high-power electron accelerators, such as the 35 MeV, 120 kW linac from MEVEX Corp (Stittville, ON, Canada) or the Rhodotron TT300-HE. The latter is an electron accelerator characterized by a maximum energy of 40 MeV and a beam power up to 125 kW, produced by IBA (Louvain-La-Neuve, Belgium). Accurate knowledge of interaction cross-sections is crucial for scalable production of medical radionuclides. At the Bern University Hospital's medical cyclotron facility, cross-sections of several proton-induced nuclear reactions were measured, in particular those involving the production of so-called theranostic pairs, such as ^{43,44}Sc/^{47}Sc, ^{61,64}Cu/^{67}Cu and ^{152,155}Tb/^{149,161}Tb, as well as more recently of the Auger emitter ^{165}Er that can be potentially be used in combination with other lanthanides (Dellepiane et al., 2022b,c, 2023c,b, 2022a, 2023a). Currently, we are investigating the feasibility of the METAS electron microtron (maximum energy: 22 MeV, average current: 20 μA) for studying selected photonuclear reactions, in particular for the production of ^{225}Ac $\left[t_{1/2} = 9.9\ \mathrm{d}, E_\alpha = 5.8\ \mathrm{MeV}(100\%)\right]$, ^{47}Sc [$t_{1/2}$ = 3.349 d, $E^{max}_{\beta^-}$ = 440.9 keV(68.4%); 600.3 keV(31.6%), E_γ = 159.4 keV(68.3%)], and ^{67}Cu [$E^{max}_{\beta^-}$ = 377 keV(57%); 468 keV(22%); 562 keV(20%)].

In particular, ^{225}Ac is emerging as one of the most promising radionuclides for Targeted Alpha Therapy (TAT). Recent studies have demonstrated the remarkable potential of ^{225}Ac-PSMA-617 for prostate cancer therapy (Kratochwil et al., 2020). However, the current availability of ^{225}Ac is insufficient to meet the high demand for clinical applications. The main production routes include the radiochemical extraction from ^{229}Th, high-energy proton induced spallation of ^{232}Th and ^{238}U targets (Robertson et al., 2019), and neutron irradiation of ^{232}Th and ^{226}Ra targets (Hoehr et al., 2017). A viable, but not yet fully studied alternative route for the production of ^{225}Ac in large scale is the irradiation of ^{226}Ra targets with high-energy gamma rays (Melville et al., 2007). Considering the assessment of the ^{226}Ra(γ, n)^{225}Ra cross-section, we aim to establish a rigorous procedure for the measurement of photonuclear reactions at METAS. This paper details the validation of this procedure through the measurement of a well-established photonuclear monitor reaction, namely the ^{197}Au(γ, n)^{196}Au reaction (Thiep et al., 2006; Veyssiere et al., 1970; Itoh et al., 2011). The Methods section outlines the microtron accelerator at METAS, the processes of irradiation and measurements, Monte Carlo simulations, and data analysis techniques. The results are presented and discussed in the subsequent two sections, culminating in a conclusion and an outlook for future work.

2. Materials and methods

After describing the electron accelerator at METAS in the first subsection, the irradiation procedures and the measurements with gamma spectroscopy are discussed in the second subsection. The third subsection focuses on the assessment of the photon fluence spectrum through Monte Carlo simulation. Finally, the data analysis techniques are discussed.

2.1. The accelerator at METAS

The irradiation experiments were conducted at the electron accelerator of the Swiss Federal Institute of Metrology (METAS). The accelerator is of microtron type, capable of producing electron beams with an endpoint energy from 4 MeV to 22 MeV. The installed accelerator is based on the design described in Svensson et al. (1977).

The relevant parts of the accelerator facility are shown in Fig. 1. The initial electron beam is formed in an electron gun and is accelerated inside a resonator (535 keV per revolution). The electron beam cycles through the resonator, by a constant magnetic field, until the extraction tube offsets its path. Subsequently, the electron beam enters the beamline. Here the beam is shaped by four quadrupole magnets (QM1 to 4) and four steering magnets (SM1 to 4), and transported via two bending magnets (BM1 and 2) to the treatment head. The beam is extracted from the vacuum tube to air through a 400 μm thick aluminium window and directed onto a converter target. A gold plate (2 mm thick with a diameter of 10 mm) acts as a Bremsstrahlung converter. Thermal cooling of the converter is provided by a copper housing, through which water is circulated. Water and copper located behind the gold disc (in the beam direction) absorb residual emerging electrons and low-energy photons, hence hardening the photon beam. A tungsten block with a conical opening acts as a collimator. Under normal operation conditions, the photon energy spectrum would be further shaped by a flattening filter located downstream of the collimator. The filters are interchangeable by a revolver assembly. For our irradiations, the flattening filter was replaced by a custom target mount, described in Section 2.2.

A single electron beam pulse has a duration of 3 μs and a current of 25 mA to 100 mA (depending on beam energy). The repetition rate can be varied step-wise in the range of 1 Hz and 200 Hz. On the converter, the beam is assumed to have a Gaussian shape with a full width at half maximum (FWHM) of 3 mm. Although every electron orbit in the accelerator can be accessed by the extraction tube, optimized magnet settings only exist for a subset of orbits. The exact energy corresponding to an orbit, as well as the energy spread within an orbit, was determined using a magnetic spectrometer in a separate beamline, dedicated for total absorption dosimetry (Vörös et al., 2012). The energy spread was found to be of the order of 25 keV for all measured orbits.

2.2. Irradiation and measurements

To validate the proposed experimental procedure with the measurement of a well-established photonuclear cross section, we selected the ^{197}Au(γ, n)^{196}Au reaction. Gold foils with a diameter of 25 mm and a nominal thickness of 12.5 μm have been purchased from Goodfellow, GmbH. We performed irradiation runs of 10 gold targets at different electron energies in the range 8.499–20.678 MeV. It should be noted that the energy threshold of the ^{197}Au(γ, n)^{196}Au nuclear reaction is 8.070 ± 0.003 MeV (Audi et al., 2003). To evaluate the initial number of target nuclei, each gold foil was weighted prior to the irradiation using a precision scale[1] with a typical uncertainty of 0.007 mg. Irradiation times were chosen based on the predicted activity and ranged from half an hour (for the irradiation at the highest beam energy) to 6 h (for the irradiation at the lowest beam energy). The charge of each individual beam pulse was measured using an AC current transformer (ACCT)[2] connected to a high bandwidth waveform digitizer.[3] For each irradiation, individual pulses were recorded and summed post-irradiation to obtain the total charge on the Bremsstrahlung converter. This current/charge measurement setup was calibrated against a Faraday Cup. Comparing the simultaneously collected charge in the Faraday cup over a precision resistor (50 Ω) to the area of the ACCT signal allowed to obtain a linear calibration curve over the range of 25 nC to 225 nC. Thus, establishing an accurate charge measurement for individual pulses. The calibration curve is shown on the left in Fig. 2, on the right-hand side of the figure a typical evolution of the beam current during an irradiation

[1] Mettler Toledo XP205
[2] Bergoz ACCT-S-055
[3] Spectrum Instrumentation, M2p5962-x4

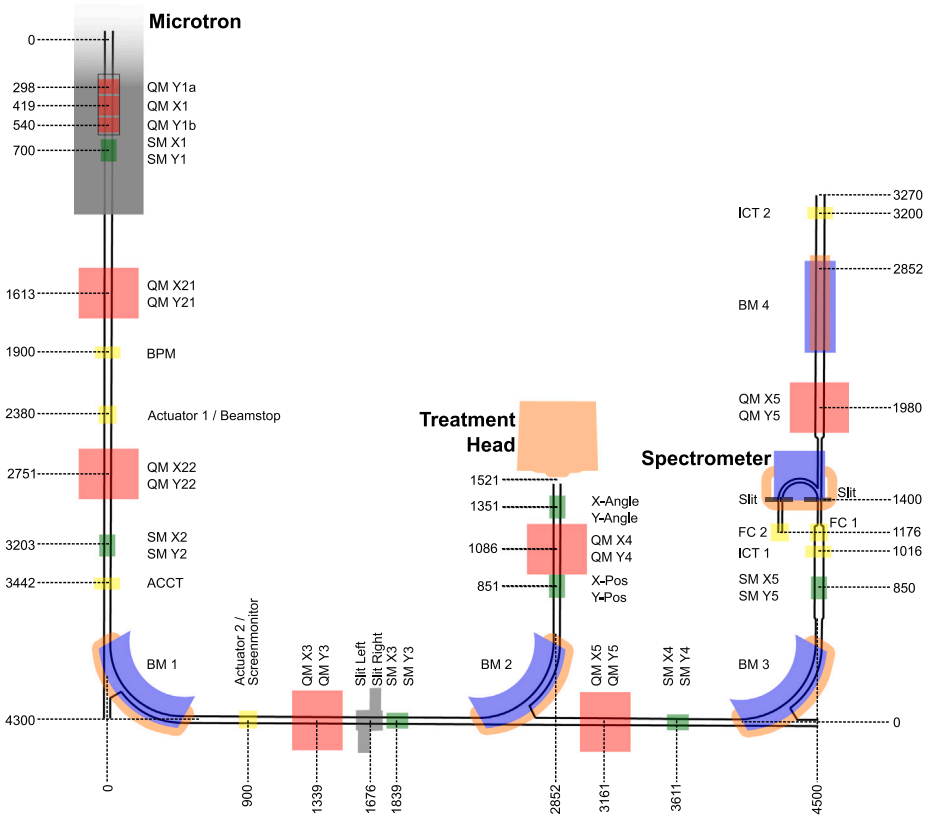

Fig. 1. Scheme of the main elements of the Microtron accelerator facility at METAS. Quadrupole magnets are depicted in red, steering magnets in green and bending magnets in blue. Instrumentation in shown in yellow.

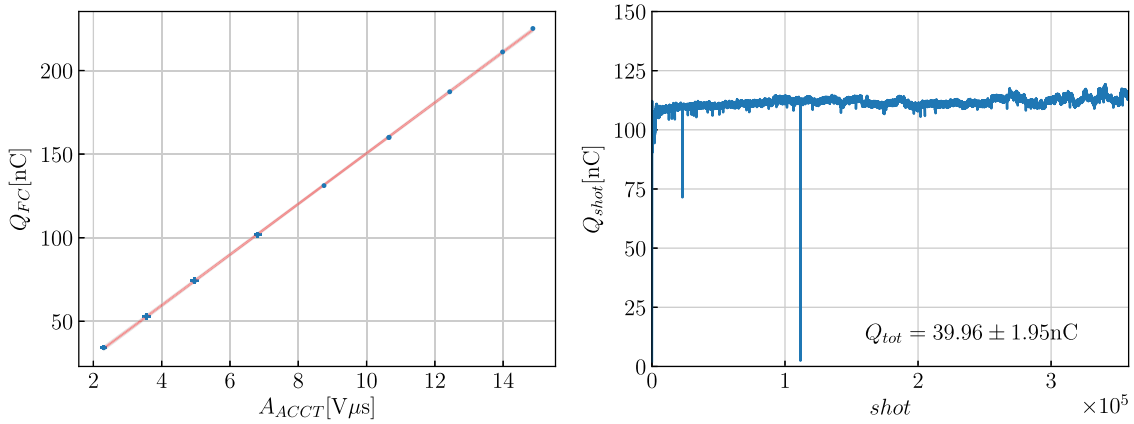

Fig. 2. The left hand side show the calibration curve of the recorded ACCT area against the charge collected in the Faraday cup. The right hand side shows the beam charge evolution over the entire irradiation with a beam energy of 20.678 MeV.

is shown. To investigate the stability of the calibration, the calibration factors were monitored for various beam repetition rates and vertical and horizontal displacements (using steering magnets SM X2 and Y2 until the beam was lost). Based on these investigations, the uncertainty of the beam charge was quantified to be within 1.2 %.

EBT3 Gafchromic films were used to evaluate the photon beam uniformity in the position of the gold foil (Casolaro et al., 2019). The beam was found to be uniform within 1% on the foil surface. The activity of the gold targets at the end of the irradiation was measured with a High Purity Germanium (HPGe) detector in operation at the cyclotron laboratory of the University of Bern. The detector's energy calibration and efficiency are periodically verified with a multi-peak radioactive source type EG 3X from EUROSTANDARD CZ, spol. s r.o., with an energy resolution of 0.24% (^{137}Cs peak FWHM). The detector is used on a daily basis for cross section, activity, and half-life measurements of radionuclides of medical interest (Dellepiane et al., 2021; Juget et al., 2023; Durán et al., 2022). The detector is a coaxial N-type HPGe (Canberra GR2009) with the sensitive volume shielded by 10 cm of lead. The pre-amplifier signal is fed into a Lynx digital analyser. The gamma spectra were analysed using the Interspec software (Johnson et al., 2021). As an example, Fig. 3 shows the gamma spectrum of a gold target after exposure to the Bremsstrahlung beam.

The energies of all the peaks related to the ^{196}Au decay are highlighted, whereas the inset zooms on the peaks used in the analysis, namely the 355.73 keV (87.0%) and the 333.03 keV (22.9%). The

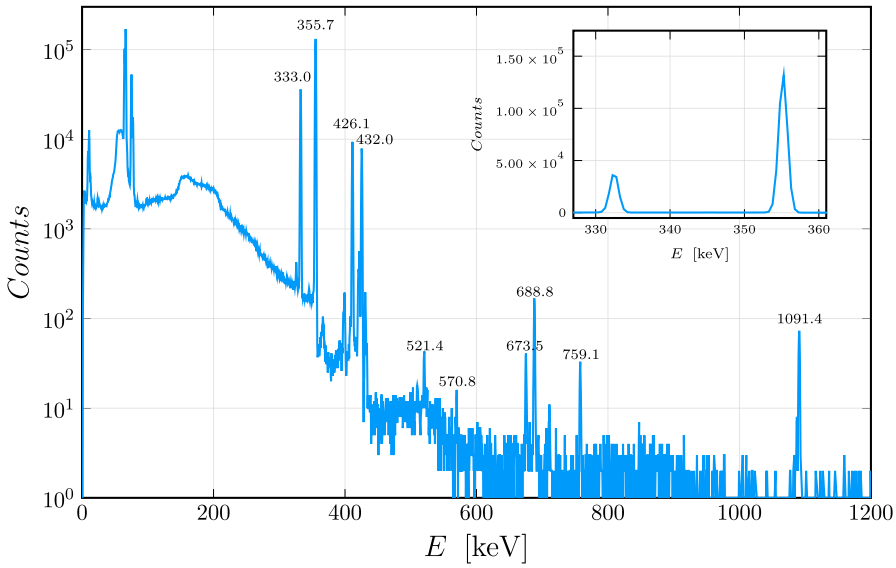

Fig. 3. Typical gamma energy spectrum of an irradiated gold target after irradiation.

Table 1
Measurement data for the available beam energies at METAS. E_{beam} is the electron beam energy, t_{irr} the duration of the irradiation, Q is the total electron charge, t_{dec} is the time between the end of irradiation and the HPGe measurement, m_{Au} is the target foil's weight and A is the measured ^{196}Au activity. The uncertainties of the beam energy and the mass are 25 keV and 0.01 mg respectively, whereas the uncertainty of the irradiation and decay times are negligible.

E_{beam} [MeV]	t_{irr} [s]	Q [mC]	t_{dec} [s]	m_{Au} [mg]	A [kBq]
8.499	21 660	1130.8 ± 13.6	25 200	123.09	(76.0 ± 8.4) · 10^{-3}
9.030	24 180	788.4 ± 9.4	19 920	122.88	1.22 ± 0.12
10.101	16 980	544.2 ± 6.5	148 860	117.45	4.35 ± 0.41
10.634	11 220	817.4 ± 9.8	7800	128.41	15.8 ± 1.5
12.228	63 380	639.7 ± 7.7	9120	123.09	48.1 ± 4.4
13.801	14 700	522.9 ± 6.2	7860	119.59	125.0 ± 11.0
15.383	3600	308.8 ± 3.7	15 180	118.07	163.0 ± 15.0
16.977	8760	193.9 ± 2.3	336 120	116.81	112.0 ± 10.0
18.562	3900	96.0 ± 1.2	24 300	127.45	128.0 ± 12.0
20.678	1860	39.9 ± 0.5	26 940	124.49	72.5 ± 6.6

mass of the gold targets, the irradiation time and the ^{196}Au activity are reported in Table 1 for all the beam energies.

2.3. Monte Carlo simulations

A key ingredient for measuring photonuclear cross sections is the precise characterization of the photon beam. Nowadays, the gold standard for assessing particle fluences in accelerator environments are Monte Carlo (MC) particle transport simulations of the relevant accelerator elements. In our case, this means simulating the accelerator head with the converter, collimators, and target assembly. We implemented the accelerator head's geometry in FLUKA version 4.0 and Flair 3.1 (Ahdida et al., 2022; Battistoni et al., 2015, 2016; Vlachoudis, 2009) based on the technical drawings of the treatment head. Fig. 4 shows Flair's rendering of the accelerator head with the vacuum window, converter with mount and cooling channels, collimators, and target. The full beam line is not part of the simulation, as it is not relevant for our purposes. The initial electron beam of the simulation starts in the vacuum pipe, just before going through the vacuum window. The electron beam shape is Gaussian in the two directions perpendicular to the beam axis, with a FWHM of 3 mm. Furthermore, the beam energy profile is implemented as Gaussian with a FWHM of 25 keV.

Fig. 5 shows the differential photon fluence for different electron beam energies. Due to the accelerator setup, a standard Bremsstrahlungs fluence spectrum is expected. The simulations run for a sufficient number of primaries to keep the statistical error on the differential photon fluence well below 1% even for photon energies close to E_{beam}.

A thorough assessment of the photon fluence's uncertainty is essential. For this purpose, we independently implemented the accelerator geometry in Geant4 (Agostinelli et al., 2003; Allison et al., 2006, 2016). Firstly, as depicted in the left plot of Fig. 6 there is excellent agreement between the Geant4 and FLUKA simulations within the statistical uncertainty (the Geant4 has a slightly higher statistical noise). This means that variations in the material definitions and in the physics implementation of electromagnetic interactions in the two codes have a negligible impact on the differential photon fluence at the target location. Secondly, our investigations revealed that significant alterations in the accelerator head's geometry are required to substantially impact the photon fluence above 5 MeV. For instance, adding a 3 cm thick polyethylene neutron moderator in front of the target merely leads to an overall reduction of ≈6% for E_{beam} = 21.74 MeV in the photon fluence at the target, as illustrated in the right plot of Fig. 6. These findings suggest that only drastic changes in geometry and material composition significantly influence the neutron fluence at the target. Moreover, replacing the water in the cooling cavity of the converter with air, a potential (temporary) failure mode not easily detected by the accelerator's monitoring system during irradiations, does not lead to a significant change in the photon fluence. Another way to asses the impact of inconsistencies between reality and simulation is the addition of a 1 mm thick lead foil directly in the photon beam between the converter and the target. Both macroscopic changes do not affect the photon fluence significantly (see right plot of Fig. 6). In conclusion, our simulation results for the fluence are robust against changes in geometry, material composition, and the physics models used in the simulation.

We also verified the simulation results experimentally with dosimetric measurements. This allows us to assess the uncertainty of the normalization of the simulations. Since the accelerator at METAS is mainly used for metrology, we performed measurements with two calibrated PTW 31014 ionization chambers inside a water phantom. The reference chamber was placed at 100 cm at a water depth of 10 g cm^{-2} from the converter directly on the central photon beam axis and the second chamber was located 7.6 cm behind. The measurements were conducted according to Anon (2020). This allowed us to verify the simulation results with two quantities: the absolute dose in the reference chamber, which provides a benchmark for the normalization of the simulation, and the ratio of the doses deposited in the two chambers, which is independent of the normalization or charge measurement

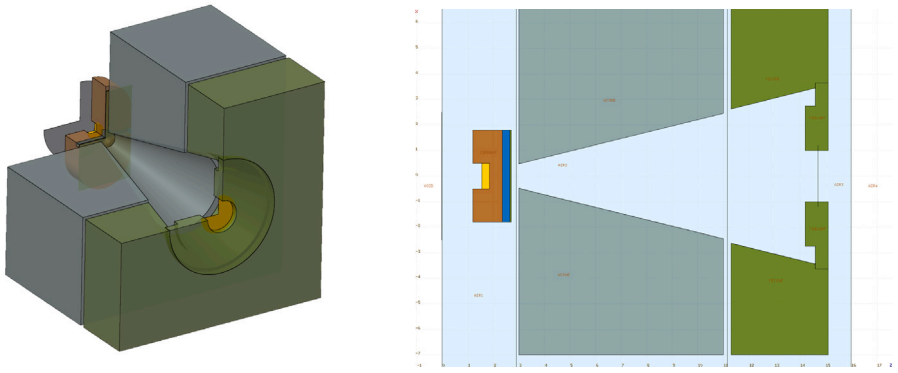

Fig. 4. FLUKA implementation of the accelerator head at METAS.

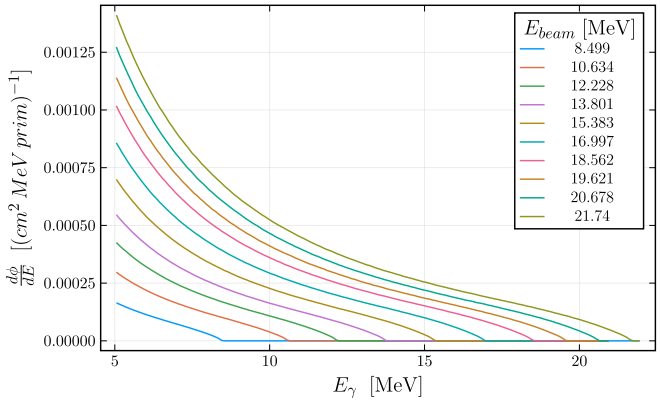

Fig. 5. Photon fluence per primary at the irradiation point from FLUKA for various beam energies.

Table 2
Comparison of the absolute dose and the ratio of dose to water in two locations between FLUKA simulations and the measured doses in PTW ionization chambers.

	D_{ref} [Gy/prim]	D_{ref}/D_{back}
FLUKA	$(8.02 \pm 0.29) \cdot 10^{-16}$	1.45 ± 0.08
PTW chamber	$(8.68 \pm 0.44) \cdot 10^{-16}$	1.43 ± 0.10

and contains information about the lower energy part of the photon spectrum.

For an electron beam energy of 15.383 MeV, Table 2 reports the dose in the reference chamber and the ratio of the doses from the two chambers. The measurements were repeated five times, which yielded a statistical error of about 3%. Furthermore, we assumed an experimental uncertainty on the beam charge measurement of 1.2%.

The FLUKA simulation of this dosimetric measurement involved a significant extension of the accelerator geometry. The irradiation target (and its support structure) was replaced by a flattening filter, manufactured of Aluminum with a conical Lead insert. Additional Tungsten collimators, consisting of four slanted blocks (arranged pairwise for horizontal and vertical collimation) with an opening angle of 5.7°, were placed after the irradiation target. These collimators produce a photon field of 100 mm by 100 mm at the entrance window of the water phantom. Additionally, after the tungsten collimators, a 20 mm thick Aluminum slab and a 10 mm high Aluminum cone (with a base radius of 110 mm and tip directed downstream of the beam) are placed in the beam path. This arrangement is designed to harden the photon spectrum by absorbing lower energy photons and secondary electrons. The water phantom (582 × 555 × 615 mm^3, (width × water height × depth in beam direction) consists of a 2.6 mm thick polystyrene beam window (160 mm by 160 mm), aligned on the beam axis and thicker PMMA walls elsewhere. The dose is scored in regions of the size of the chambers according to the PTW specifications (using regional USRBIN scoring). We show the results with the statistical uncertainty of the simulation in Table 2. The simulation results agree very well with the measurements. Although with this experimental setup, we probe primarily the lower end of the photon energy spectrum, this test measurement gives us confidence that our characterization of the photon beam with FLUKA is accurate. Especially since the generation of Bremsstrahlung is well understood and verified, see for example Faddegon et al. (2008) and references therein. If there was a significant systematic error in the simulations, the agreement between FLUKA and the measurements in Table 2 would be much worse.

The MC simulations do not only provide the differential photon fluence as the input for the cross section measurement, they also provide the yield of the activation products in the target material. This is a valuable benchmark and comparison for the experimental determination of the yield. The activation products are scored with RESNUCLE card with radioactive decay set in semi-analogue mode. Of course, the photonuclear interactions need to be turned on in FLUKA with the PHOTONUC card set to ELECTNUC (we do not need any photonuclear interactions with muons) and with the COALESCE and EVAPORAT settings of the PHYSICS card. For the target material, the same biasing factor applies as in the case of the aforementioned converter biasing.

Note that FLUKA has its own implementation of photonuclear cross sections. As described in Fassò et al. (1997, 2005) FLUKA has its own cross section library for photonuclear interactions for about 190 stable nuclides. In the energy range around the giant dipole resonance (GDR), which is relevant for our study, the photonuclear cross sections are based on an evaluated parametrization done by the FLUKA developers based on available experimental data and theoretical considerations (Fassò et al., 2005). An assessment of the systematic uncertainty on the yield of activation products in FLUKA, in particular ^{196}Au, would go beyond the scope of this work since it would mean evaluating the accuracy of the implemented cross section. We therefore only report the statistical uncertainty on the yield from FLUKA.

2.4. Data analysis

From the target irradiations at METAS, we obtained the yield of ^{196}Au in the target foil, the foil's weight and the time integrated electron beam charge. To keep all measured information separate from the modelled and/or simulation data, we normalized the measured yield of ^{196}Au to the number of primary particles and unit volume and denote it as $y_{Au}(E_{beam})$. This involves the decay correction for the time between the irradiation of the target and its HPGe measurement. We assume a decay constant for ^{196}Au of $\lambda = (1.3009 \pm 1.27 \cdot 10^{-4}) \cdot 10^{-6}\ s^{-1}$ according to Xiaolong (2007).

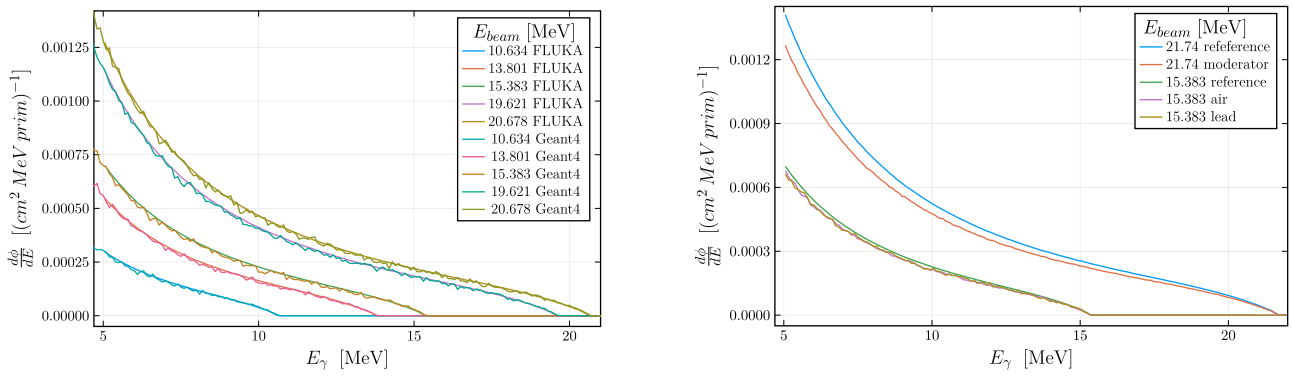

Fig. 6. Comparison between the photon fluence from Geant4 and FLUKA (left) and impact of geometry alterations in the FLUKA simulations (right).

The relation of $y_{Au}(E_{beam})$ to the production cross section and photon fluence ϕ is given by the following integral over the respective energy range

$$y_{Au}(E_{beam}) = \rho_{Au} \int_{E_{th}}^{E_{beam}} \frac{d\phi(E_{beam}, E)}{dE} \cdot \sigma(E)\, dE\,. \tag{1}$$

Where E_{th} is the threshold energy, ρ_{Au} is the number density of target nuclei, and σ is the photonuclear cross section for $^{197}\mathrm{Au}(\gamma, n)\,^{196}\mathrm{Au}$. With the differential photon fluence determined through the FLUKA simulation, it is possible to extract the cross section σ from the measured yields $y_{Au}(E_{beam})$.

The limited number of available electron beam energies implies several restrictions. On the one hand, we had to restrict the shape of σ to a truncated Breit-Wigner function

$$\sigma(E) = \frac{n \cdot k \cdot \Theta(E - E_{th})}{(E^2 - m^2)^2 + m^2\,\Gamma^2}\,, \quad \text{with} \quad k = \frac{2\sqrt{2}}{\pi} \frac{m \cdot \Gamma \sqrt{m^2(m^2 + \Gamma^2)}}{\sqrt{m^2 + \sqrt{m^2(m^2 + \Gamma^2)}}}\,. \tag{2}$$

The threshold energy E_{th} for the $^{197}\mathrm{Au}(\gamma, n)\,^{196}\mathrm{Au}$ reaction is fixed to 8.070 ± 0.003 MeV according to Audi et al. (2003). n is a normalization constant which is fitted to the measured data together with the mass m and width Γ of the GDR.

At energies around the GDR, this is an appropriate model for the cross section in the case of gold. Note that for non-spherical nuclei the cross section might be a combination of two Breit-Wigner functions and also the $\sigma \propto \sqrt{E - E_{th}}$ behaviour in the threshold region is not implemented in Eq. (2). Given the limited number of data points, fitting a more complex parametrization of σ is bound to fail.

We performed a Bayesian fit of the parameters n, m, and Γ using the Turing.jl package (Bezanson et al., 2017; Ge et al., 2018). We believe that the integral in Eq. (1) and the limited number of data points make a Bayesian approach more appropriate. A Gaussian likelihood and the following conservative priors were used for the fitting procedure

$$\begin{aligned} n &\sim \mathcal{N}(10^{-24}\,\mathrm{cm}^2, 10^{-24}\,\mathrm{cm}^2)\,, \\ m &\sim \mathcal{N}(14.0\,\mathrm{MeV}, 3.0\,\mathrm{MeV})\,, \\ \Gamma &\sim \mathcal{N}(2.0\,\mathrm{MeV}, 1.0\,\mathrm{MeV})\,. \end{aligned} \tag{3}$$

In addition, the statistical noise has a normally distributed prior. All of the priors' normal distribution were truncated at 0. Since the calculation of the posterior distribution requires numerous evaluations, the integral in Eq. (1) is performed using the trapezoidal rule. Given the small bin size of the photon fluence of 0.1 MeV and the smoothness of the integrand function, we assume that the uncertainty on the numerical evaluation of the integral is marginal.

In our analysis, we did not assume any uncertainty on the differential photon fluence from the FLUKA simulations. With the checks described in the previous section, the shape and the normalization of $d\phi/dE$ are well under control. Furthermore, any normalization uncertainty would simply propagate into the parameter n when sampling the posterior distribution. Moreover, changes in the shape of the photon fluence spectrum, e.g. introducing a bin-wise error, are hardly noticeable due to the integration in Eq. (1).

From Eq. (1) and the shape of the Breit-Wigner function, it is clear that the fit results are mostly dependent on the data points with E_{beam} below the peak of the GDR (see also Nair et al., 2008), i.e. in our case $E_{GDR} = 13.7$ MeV (Xiaolong, 2007). It was therefore our primary goal to get as much data points in this energy range to improve the fit as much as possible.

3. Results

In Table 1 we present the measured ^{196}Au yields together with the irradiation data. The data was taken with different target foils and therefore the target's mass was added. Due to the long irradiation time and long half-life of ^{196}Au, it is safe to assume a negligible uncertainty on t_{irr} and t_{dec}. The uncertainty on the target mass measurement is also negligible. The electron beam energy is restricted to a narrow energy range due to the stability criterion of the accelerator design. Additionally, beam energies for individual orbits were determined during commissioning of the accelerator using a magnetic spectrometer (see Fig. 1). Here, the energy spread of the electron beam was also measured to be 25 keV. A statistical uncertainty on the number of counts measured with the HPGe was considered for the ^{196}Au activity(Table 1).

Fig. 7 shows the decay-corrected and normalized yield from the measurements in comparison with the simulated yield. The uncertainty on the decay constant of ^{196}Au, retrieved from National Nuclear Data Center, is negligible. Only at lower energies, close to the $^{197}\mathrm{Au}(\gamma, n)\,^{196}\mathrm{Au}$ reaction threshold, the measured and the simulated yields do not agree well. On the one hand, the measurements in this regime are plagued by long irradiation times and low activities. On the other hand, FLUKA has its own evaluated cross section library and the implementation of the $^{197}\mathrm{Au}(\gamma, n)\,^{196}\mathrm{Au}$ reaction threshold is not disclosed. Note that standard evaluated cross section libraries like TENDL (Koning et al., 2019) and IAEA (Kawano et al., 2020) differ at threshold energies.

The error bars on the FLUKA yield in Fig. 7 are hardly visible. The statistical errors are 7.8% and 3.8% for the two lowest beam energies and well below 1% for the higher beam energies. The measured yield's error is given only by the uncertainty of the HPGe measurement and is around 10% (see also Table 1). The fit prediction from the measurement data is also shown in Fig. 7.

Table 3 shows the fit results for the measured and simulated yield, respectively. The fit to the FLUKA data provides a useful check for the fitting procedure in the absence of any experimental uncertainty. The parameter's pdf are Gaussian, as can be seen in Fig. 9. The 95% credible intervals for the measured parameters that correspond to the

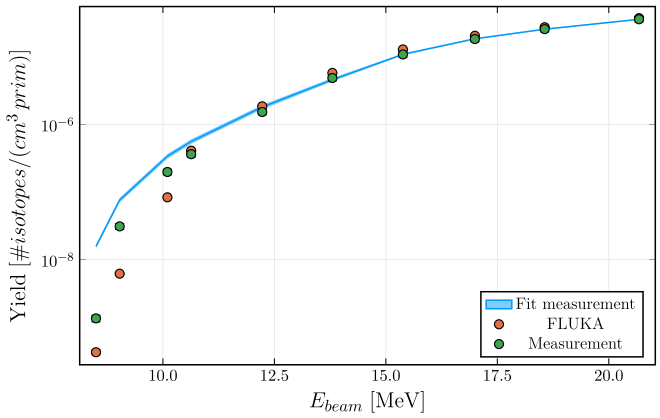

Fig. 7. Comparison of the ^{196}Au yield per primary beam particle, i.e. electrons, between FLUKA and the measured data. The blue band shows the yield predicted by the measurement's cross section fit.

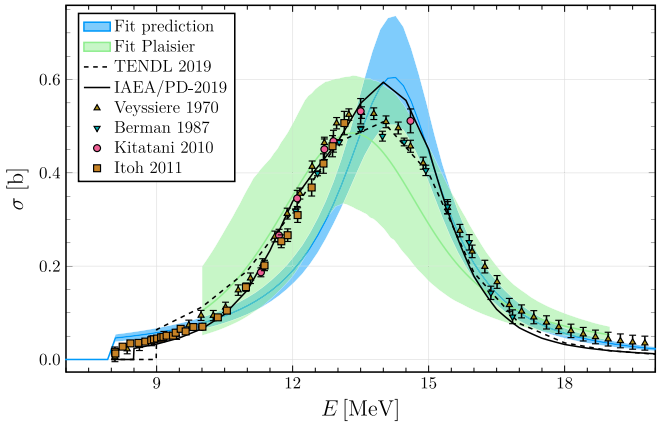

Fig. 8. ^{197}Au$(\gamma, n)^{196}$Au cross section from the measured data fit (see Table 3) in comparison with the model cross sections from TENDL 2019 (Koning et al., 2019), ENDF/B-VII.0 (Chadwick et al., 2006), IAEA 2019 (Kawano et al., 2020) and Plaisir et al. (2012). Also shown are the experimental cross sections of Berman et al. (1987), Veyssiere et al. (1970), Itoh et al. (2011) and Fumito et al. (2010).

Table 3
Results from fitting the Breit-Wigner function of Eq. (2) to either the FLUKA or measured ^{196}Au yield. The parameter's pdf is shown in Fig. 9.

	n [10^{-24} cm^2]	m [MeV]	Γ [MeV]	ε [$\#iso/(\mathrm{cm}^3 prim)$]
FLUKA	2.43 ± 0.04	13.5 ± 0.1	2.12 ± 0.20	$(1.70 \pm 0.60) \cdot 10^{-7}$
Measurement	2.58 ± 0.05	14.2 ± 0.1	2.76 ± 0.27	$(2.28 \pm 0.81) \cdot 10^{-7}$

standard deviations given in Table 3, are $[2.48, 2.68] \cdot 10^{-24}$ cm^2 for n, [14.0, 14.40] MeV for m and [2.23, 3.29] MeV for Γ, respectively. Clearly, the uncertainties on the parameters of the Breit-Wigner function are relatively small.

Finally, Fig. 8 shows the resulting ^{197}Au$(\gamma, n)^{196}$Au cross section from the measured yield. The peak of the cross section from the measurement is slightly shifted towards higher energies in comparison with the fitted cross section from FLUKA (see also parameter m in Table 3). However, the evaluated cross sections from Koning et al. (2019), Kawano et al. (2020) have the peak well within the error band of the measurement fit.

4. Discussion

The results from fitting a Breit-Wigner curve to the measured ^{196}Au yield in Table 3 show that the methodology discussed in Section 2 allows to determine photonuclear cross sections with the electron accelerator at METAS. For the reference process ^{197}Au$(\gamma, n)^{196}$Au, the uncertainties on the predicted cross section in Fig. 8 are consistent with the experimental and evaluated cross sections from the literature in the ranges 8 MeV-11 MeV and 14 MeV-22 MeV. The observed difference in the range 11 MeV-14 MeV is due to the limited number of experimental points, in particular near the reaction threshold, and from the use of a symmetric Breit-Wigner function for the fitting procedure. This aspect is both a limitation and a strength of our experimental approach. Indeed, our method can be effectively used to measure unknown experimental cross sections providing critical information on key parameters such as the cross-section peak. Fig. 9 demonstrates how the fit strongly reduced the width of the posterior pdf compared to the priors. Therefore, there is a significant gain in information over our prior knowledge. To improve accuracy, it is desirable to use alternative experimental methods, such as those using quasi-monochromatic gamma rays (e.g., from inverse Compton scattering of laser photons) and performing direct measurements of recoil neutrons, as reported in Thiep et al. (2006).

Unsurprisingly, the fit is mostly sensitive to the yield values around the resonance peak. In this region, the Breit-Wigner curve has the strongest gradient and the photon fluence is still large. Therefore, slight changes in the upper integration limit in Eq. (1) have a larger impact on the yield.

Given the multiple orders of magnitude of the measured and simulated yields, it might be tempting to perform the fit in log space. The $\log(y_{Au})$ has a high gradient at low energies and flattens towards $\sim$ 20 MeV. Fitting the log of the yield therefore gives a higher weight to the lower energy data points. The measured points in the threshold region are, however, affected by low count statistics and therefore may be affected by systematic uncertainties. Furthermore, the convergence of the fit worsens in log space and the relative errors on n, m and Γ increase compared to the results in Table 3.

Comparing the fits to the measured and simulated yields, it is clear that there is an underestimation of the yield starting around 11 MeV. This is the reason why the FLUKA data leads to a higher peak of the Breit-Wigner curve (see Table 3). Interestingly, these lower values of the yield do not drive m to higher energies. This is because close to the threshold energy, the simulated yield is lower compared to the measured one. Additionally, we can compare our fit results to Plaisir et al. (2012). In this study, the experimental method aligns with our approach, involving Bremsstrahlung irradiation and subsequent activation measurement. The main divergence lies in the setup geometry. However, the data analysis methods differ significantly; the authors employed a χ^2 minimization of a two Lorentzian model to extract the cross section from yield measurements. In Fig. 8, we have depicted the fit and its associated confidence interval for this model. The sizeable confidence interval primarily arises from a 5 % uncertainty in most of the parameters. Notably, our results are consistent with this study across the entire energy range. When compared to the evaluated data from IAEA/PD-2019 (Kawano et al., 2020), the TENDL 2019 model (Koning et al., 2019), and available experimental data from both positron annihilation (Berman et al., 1987; Veyssiere et al., 1970) and laser Compton scattering experiments (Itoh et al., 2011; Fumito et al., 2010), our results align well concerning the slope and position of the higher energy lobe of the cross-section peak. Additionally, the peak location concurs with the most recent evaluated data published in the IAEA/PD-2019 report. Unfortunately, no experimental data covering the entire energy range of the GDR from this report are available for comparison. However, it becomes evident that on the low-energy side, our estimation of the cross-section is lower than other models and experimental data (Berman et al., 1987; Veyssiere et al., 1970; Itoh et al., 2011; Fumito et al., 2010). This disparity stems from the overestimation of the peak amplitude and the underestimation of the peak width (as discussed further below regarding parameter correlations).

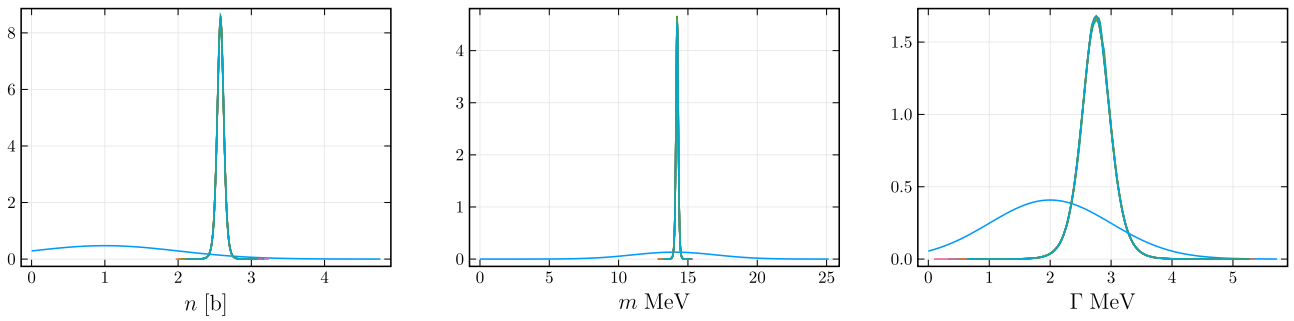

Fig. 9. Comparison of the prior (blue) and posterior (green) pdf for the three fitting parameters n, m and Γ. The measurement data constrains the parameter rather strongly.

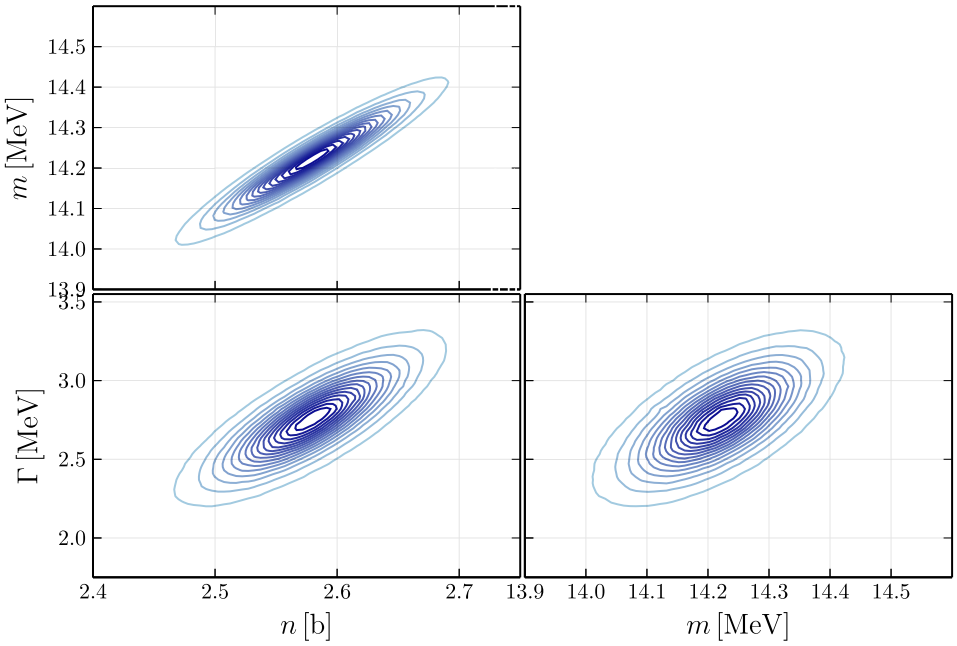

Fig. 10. Pair plot of the three parameters for the fit to the measured yield showing a strong correlation of the posterior distributions.

Fig. 10 presents the pair plot of the fitting parameters for the case of the measured data. Clearly, the parameters n, m and Γ are strongly correlated with each other. This stems from the integration in Eq. (1) since it averages out the Breit-Wigner curve. Increasing the normalization n will drive m towards higher energies to decrease the overlap between the peak of the Breit-Wigner curve and the high fluence region. The same reasoning works for the other two correlations, i.e. higher values of m require a wider cross section that can still catch higher fluence contributions at lower energies and increasing n makes the Breit-Wigner function flatter.

The number of beam energies, of course, limits the goodness of the fit. As a cross check, we simulated more beam energies and performed a fit of the resulting yield. This means we effectively reverse engineered the cross section implemented in FLUKA. With a total of 18 beam energies, of which 12 lied below 14 MeV, the parameters are constrained much stronger. Even for Γ the relative error drops below 1%. This shows that despite the averaging of the integral in Eq. (1) the method can improve with more data points. The degeneracies of the parameters from Fig. 10 remain.

Despite the good results for the $^{197}\mathrm{Au}(\gamma,n)^{196}\mathrm{Au}$ cross section, our method and experimental setup face some challenges. On one side there is a model dependence in the sense that we need to rely on the assumption of a Breit-Wigner shape of the cross section. This assumption should be questioned in particular when measuring cross sections with non-spherical target nuclei that require more complex fitting functions. Increasing the number of fitting parameters, such as e.g. if the sum of two Breit-Wigner functions, would certainly require additional data points to keep the uncertainties at an acceptable level. On the other side, our method requires input from MC simulations, which could be viewed as a limitation or, at least, as a source of systematic uncertainties. A good characterization of the experimental setup and verification of the MC simulations (see also Section 2) is therefore key for a successful determination of photonuclear reaction cross sections.

5. Conclusions and outlook

In this study, we showed that it is possible to measure the photonuclear reaction cross section for the reaction $^{197}\mathrm{Au}(\gamma,n)^{196}\mathrm{Au}$ using the Microtron at METAS. The ^{196}Au yield in thin gold foils is determined by irradiating thin gold foils with photons and measuring the induced activity with a HPGe spectrometer. Assuming that the cross section follows a Breit-Wigner curve and with the modelling of the photon fluence using MC simulations, we were able to reproduce the reference values for the $^{197}\mathrm{Au}(\gamma,n)^{196}\mathrm{Au}$ cross section through a Bayesian fitting procedure. Even with a limited number of beam energies, the Bayesian fitting procedure yields low uncertainties on the parameters of the Breit-Wigner shape of the cross section. Our results crucially rely on an accurate characterization of the photon fluence spectrum, as well as on the precise determination of the induced activity and the electron

beam current. The method presented in this study can be translated easily to other photonuclear reactions, for which the cross sections are hardly known. Depending on the process under investigation, more fitting parameters will be required (sum of two Breit-Wigner functions or multi-isotopic target materials). Therefore, we envision that more beam energies would be required for more complex fits to the data. The isotope ^{226}Ra is an intriguing candidate. The cross-section for this reaction would be interesting, considering large-scale production of ^{225}Ac for targeted alpha therapy using the photonuclear route. With the presented methodology, we laid the groundwork to accurately measure photonuclear cross sections with a relatively simple setup. The method can be easily applied at other facilities which might have access to higher beam energies or higher beam currents.

In sum, our study not only validates the methodology for measuring the photonuclear reaction cross section using the ^{197}Au$(\gamma, n)^{196}$Au reaction, but also opens up new avenues for extending this approach to other isotopes and applications.

Funding

This study is supported by Swiss National Science Foundation Sinergia grant PHOtonuclear Reactions (PHOR): breakthrough research in radionuclides for theranostics awarded to A. Türler, S.Braccini and C. Kottler; Schweizerischer Nationalfonds zur Förderung der Wissenschaftlichen Forschung (CRSII5_180352).

CRediT authorship contribution statement

Saverio Braccini: Writing – review & editing, Supervision, Project administration, Funding acquisition. **Pierluigi Casolaro:** Writing – review & editing, Writing – original draft, Visualization, Validation, Software, Methodology, Investigation, Formal analysis, Data curation, Conceptualization. **Gaia Dellepiane:** Writing – review & editing, Investigation. **Christian Kottler:** Writing – review & editing, Supervision, Project administration. **Matthias Lüthi:** Writing – review & editing, Writing – original draft, Visualization, Validation, Software, Methodology, Investigation, Formal analysis, Data curation, Conceptualization. **Lorenzo Mercolli:** Writing – review & editing, Writing – original draft, Visualization, Validation, Software, Methodology, Investigation, Formal analysis, Data curation. **Peter Peier:** Writing – review & editing, Supervision. **Paola Scampoli:** Supervision. **Andreas Türler:** Writing – review & editing, Project administration, Funding acquisition.

Declaration of competing interest

The authors declare that they have no known competing financial interests or personal relationships that could have appeared to influence the work reported in this paper.

Data availability

Data and source code is available under https://doi.org/10.5281/zenodo.10790863.

References

Agostinelli, S., Allison, J., Amako, K., Apostolakis, J., Araujo, H., Arce, P., Asai, M., et al., 2003. Geant4—a simulation toolkit. Nucl. Instrum. Methods Phys. Res. A 506 (3), 250–303. http://dx.doi.org/10.1016/S0168-9002(03)01368-8.

Ahdida, C., et al., 2022. New capabilities of the FLUKA multi-purpose code. Front. Phys. 9, 788253. http://dx.doi.org/10.3389/fphy.2021.788253.

Allison, J., Amako, K., Apostolakis, J., Araujo, H., Arce Dubois, P., Asai, et al., 2006. Geant4 developments and applications. IEEE Trans. Nucl. Sci. 53 (1), 270–278. http://dx.doi.org/10.1109/TNS.2006.869826.

Allison, J., Amako, K., Apostolakis, J., Arce, P., Asai, M., Aso, T., et al., 2016. Recent developments in geant4. Nucl. Instrum. Methods Phys. Res. A 835, 186–225. http://dx.doi.org/10.1016/j.nima.2016.06.125.

Anon, 2020. Procedures of dosimetry with probe-type detectors for photon and electron radiation – part 2: Ionization chamber dosimetry of high energy photon and electron radiation. In: Standard DIN 6800-2:2020-08. DIN Deutsches Institut für Normung e.V.

Audi, G., Wapstra, A.H., Thibault, C., 2003. The Ame2003 atomic mass evaluation: (II). Tables, graphs and references. Nuclear Phys. A 729 (1), 337–676. http://dx.doi.org/10.1016/j.nuclphysa.2003.11.003, the 2003 NUBASE and Atomic Mass Evaluations.

Battistoni, G., Bauer, J., Boehlen, T.T., Cerutti, F., Chin, M.P.W., Dos Santos Augusto, R., et al., 2016. The FLUKA code: An accurate simulation tool for particle therapy. Front. Oncol. 6, http://dx.doi.org/10.3389/fonc.2016.00116.

Battistoni, G., et al., 2015. Overview of the FLUKA code. Ann. Nucl. Energy 82, 10–18. http://dx.doi.org/10.1016/j.anucene.2014.11.007.

Berman, B.L., Pywell, R.E., Dietrich, S.S., Thompson, M.N., McNeill, K.G., Jury, J.W., 1987. Absolute photoneutron cross sections for Zr, I, Pr, Au, and Pb. Phys. Rev. C Nucl. Phys. 36, 1286. http://dx.doi.org/10.1103/PhysRevC.36.1286.

Bezanson, J., Edelman, A., Karpinski, S., Shah, V.B., 2017. Julia: A fresh approach to numerical computing. SIAM Rev. 59 (1), 65–98. http://dx.doi.org/10.1137/141000671.

Casolaro, P., Campajola, L., Di Capua, F., 2019. The physics of radiochromic process: one calibration equation for all film types. J. Instrum. 14 (08), P08006. http://dx.doi.org/10.1088/1748-0221/14/08/P08006.

Chadwick, M., Obložinský, P., Herman, M., Greene, N., McKnight, R., Smith, D., et al., 2006. Endf/b-vii.0: Next generation evaluated nuclear data library for nuclear science and technology. Nucl. Data Sheets 107 (12), 2931–3060. http://dx.doi.org/10.1016/j.nds.2006.11.001, evaluated Nuclear Data File ENDF/B-VII.0.

Dellepiane, G., Belver Aguilar, C., Carzaniga, T., Casolaro, P., Häffner, P., 2021. Research on theranostic radioisotope production at the bern medical cyclotron. Il nuovo cimento C 44 (4–5), 1–4. http://dx.doi.org/10.1393/ncc/i2021-21130-6.

Dellepiane, G., Casolaro, P., Favaretto, C., Gottstein, A., Grundler, P.V., Mateu, I., Renaldin, E., Scampoli, P., Talip, Z., van der Meulen, N.P., et al., 2023a. Cross-section measurement of thulium radioisotopes with an 18 MeV medical PET cyclotron for an optimized ^{165}Er production. Appl. Radiat. Isot. 110954. http://dx.doi.org/10.1016/j.apradiso.2023.110954.

Dellepiane, G., Casolaro, P., Favaretto, C., Grundler, P.V., Mateu, I., Scampoli, P., Talip, Z., van der Meulen, N.P., Braccini, S., 2022a. Cross section measurement of terbium radioisotopes for an optimized ^{155}Tb production with an 18 MeV medical PET cyclotron. Appl. Radiat. Isot. 184, 110175. http://dx.doi.org/10.1016/j.apradiso.2022.110175.

Dellepiane, G., Casolaro, P., Gottstein, A., Mateu, I., Scampoli, P., Braccini, S., 2023b. Optimized production of ^{67}Cu based on cross section measurements of ^{67}Cu and ^{64}Cu using an 18 MeV medical cyclotron. Appl. Radiat. Isot. 195, 110737. http://dx.doi.org/10.1016/j.apradiso.2023.110737.

Dellepiane, G., Casolaro, P., Mateu, I., Scampoli, P., Braccini, S., 2023c. Alternative routes for ^{64}Cu production using an 18 MeV medical cyclotron in view of theranostic applications. Appl. Radiat. Isot. 191, 110518. http://dx.doi.org/10.1016/j.apradiso.2022.110518.

Dellepiane, G., Casolaro, P., Mateu, I., Scampoli, P., Voeten, N., Braccini, S., 2022b. ^{47}Sc And ^{46}Sc cross-section measurement for an optimized ^{47}Sc production with an 18 MeV medical PET cyclotron. Appl. Radiat. Isot. 189, 110428. http://dx.doi.org/10.1016/j.apradiso.2022.110428.

Dellepiane, G., Casolaro, P., Mateu, I., Scampoli, P., Voeten, N., Braccini, S., 2022c. Cross-section measurement for an optimized ^{61}Cu production at an 18 MeV medical cyclotron from natural Zn and enriched ^{64}Zn solid targets. Appl. Radiat. Isot. 190, 110466. http://dx.doi.org/10.1016/j.apradiso.2022.110466.

Durán, M.T., Juget, F., Nedjadi, Y., Bailat, C., Grundler, P.V., Talip, Z., van der Meulen, N.P., Casolaro, P., Dellepiane, G., Braccini, S., 2022. Half-life measurement of ^{44}Sc and ^{44m}Sc. Appl. Radiat. Isot. 190, 110507. http://dx.doi.org/10.1016/j.apradiso.2022.110507.

Faddegon, B.A., Asai, M., Perl, J., Ross, C., Sempau, J., Tinslay, J., Salvat, F., 2008. Benchmarking of monte carlo simulation of bremsstrahlung from thick targets at radiotherapy energies. Med. Phys. 35 (10), 4308–4317. http://dx.doi.org/10.1118/1.2975150.

Fassò, A., Ferrari, A., Sala, P.R., 1997. Total giant resonance photonuclear cross sections for light nuclei: a database for the fluka monte carlo transport code. In: Proc. 3rd Specialists' Meeting on Shielding Aspects of Accelerators, Targets and Irradiation Facilities. p. 61.

Fassò, A., Ferrari, A., Sala, P.R., 2005. Photonuclear reactions in FLUKA: Cross sections and interaction models. AIP Conf. Proc. 769 (1), 1303–1306. http://dx.doi.org/10.1063/1.1945245.

Fumito, K., Hideo, H., Shinji, G., Hiroaki, U., Hidetoshi, A., Takeshi, K., Hiroyuki, T., Kawakatsu, Y., 2010. Measurement of the ^{80}Se(γ, n) cross section using laser-compton scattering γ-rays. J. Nucl. Sci. Technol. 47 (4), 367–375. http://dx.doi.org/10.1080/18811248.2010.9711967.

Ge, H., Xu, K., Ghahramani, Z., 2018. Turing: A language for flexible probabilistic inference. In: A. Storkey, F. Perez-Cruz (Ed.), Proceedings of the Twenty-First International Conference on Artificial Intelligence and Statistics. In: Proceedings of Machine Learning Research, vol. 84, PMLR, pp. 1682–1690, URL https://proceedings.mlr.press/v84/ge18b.html.

Hoehr, C., Bénard, F., Buckley, K., Crawford, J., Gottberg, A., Hanemaayer, V., Kunz, P., Ladouceur, K., Radchenko, V., Ramogida, C., et al., 2017. Medical isotope production at TRIUMF—from imaging to treatment. Physics Procedia 90, 200–208. http://dx.doi.org/10.1016/j.phpro.2017.09.059.

Itoh, O., Utsunomiya, H., Akimune, H., Kondo, T., Kamata, M., Yamagata, T., et al., 2011. Photoneutron cross sections for Au revisited: Measurements with laser compton scattering gamma-rays and data reduction by a least-squares method. J. Nucl. Sci. Technol. 48 (5), 834–840. http://dx.doi.org/10.1080/18811248.2011.9711766.

Johnson, W., Chan, E., Walsh, E., Morte, C., Lee, D., 2021. USDOE. http://dx.doi.org/10.11578/dc.20211202.6, Interspec v. 1.0.8, version 1.0.8.

Juget, F., Durán, T., Nedjadi, Y., Talip, Z., Grundler, P.V., Favaretto, C., Casolaro, P., Dellepiane, G., Braccini, S., Bailat, C., et al., 2023. Activity measurement of ^{44}Sc and calibration of activity measurement instruments on production sites and clinics. Molecules 28 (3), 1345. http://dx.doi.org/10.3390/molecules28031345.

Kawano, T., Cho, Y., Dimitriou, P., Filipescu, D., Iwamoto, N., Plujko, V., et al., 2020. IAEA photonuclear data library 2019. Nucl. Data Sheets 163, 109–162. http://dx.doi.org/10.1016/j.nds.2019.12.002.

Koning, A., Rochman, D., Sublet, J.-C., Dzysiuk, N., Fleming, M., van der Marck, S., 2019. TENDL: Complete nuclear data library for innovative nuclear science and technology. Nucl. Data Sheets 155, 1–55. http://dx.doi.org/10.1016/j.nds.2019.01.002, special Issue on Nuclear Reaction Data.

Kratochwil, C., Haberkorn, U., Giesel, F.L., 2020. ^{225}Ac-PSMA-617 for therapy of prostate cancer. In: Seminars in nuclear medicine, vol. 50, Elsevier, pp. 133–140. http://dx.doi.org/10.1053/j.semnuclmed.2020.02.004.

Mamtimin, M., Harmon, F., Starovoitova, V.N., 2015. Sc-47 production from titanf<apium targets using electron linacs. Appl. Radiat. Isot. 102, 1–4. http://dx.doi.org/10.1016/j.apradiso.2015.04.012.

Maslov, O.D., Sabel'nikov, A.V., Dmitriev, S.N., 2006. Preparation of ^{225}Ac by ^{226}Ra(γ, n) photonuclear reaction on an electron accelerator, MT-25 microtron. Radiochemistry 48 (2), 195–197. http://dx.doi.org/10.1134/s1066362206020184.

Melville, G., Meriarty, H., Metcalfe, P., Knittel, T., Allen, B., 2007. Production of Ac-225 for cancer therapy by photon-induced transmutation of Ra-226. Appl. Radiat. Isot. 65 (9), 1014–1022. http://dx.doi.org/10.1016/j.apradiso.2007.03.018.

Nair, C., Erhard, M., Junghans, A.R., Bemmerer, D., Beyer, R., Grosse, E., Klug, J., Kosev, K., Rusev, G., Schilling, K.D., Schwengner, R., Wagner, A., 2008. Photoactivation experiment on ^{197}Au and its implications for the dipole strength in heavy nuclei. Phys. Rev. C 78, 055802. http://dx.doi.org/10.1103/PhysRevC.78.055802.

National Nuclear Data Center, information extracted from the NuDat database (accessed 08/2023). URL https://www.nndc.bnl.gov/nudat/.

Plaisir, C., Hannachi, F., Gobet, F., Tarisien, M., Aléonard, M., Méot, V., Gosselin, G., Morel, P., Morillon, B., 2012. Measurement of the ^{85}Rb (γ, n) ^{84m}Rb cross-section in the energy range 10-19 MeV with bremsstrahlung photons. Eur. Phys. J. A 48 (5), 68. http://dx.doi.org/10.1140/epja/i2012-12068-7.

Rane, S., Harris, J.T., Starovoitova, V.N., 2015. ^{47}Ca Production for ^{47}Ca/^{47}Sc generator system using electron linacs. Appl. Radiat. Isot. 97, 188–192. http://dx.doi.org/10.1016/j.apradiso.2014.12.020.

Robertson, A.K., Lobbezoo, A., Moskven, L., Schaffer, P., Hoehr, C., 2019. Design of a thorium metal target for ^{225}Ac production at TRIUMF. Instruments 3 (1), 18. http://dx.doi.org/10.3390/instruments3010018.

Starovoitova, V.N., Tchelidze, L., Wells, D.P., 2014. Production of medical radioisotopes with linear accelerators. Appl. Radiat. Isot. 85, 39–44. http://dx.doi.org/10.1016/j.apradiso.2013.11.122.

Svensson, H., Jonsson, L., Larsson, L.-G., Brahme, A., Lindberg, B., Reistad, D., 1977. A 22 Mev microtron for radiation therapy. Acta Radiol., Ther. Phys. Biol. 16 (2), 145–156. http://dx.doi.org/10.3109/02841867709134308.

Thiep, T.D., An, T.T., Vinh, N.T., Cuong, P.V., Belov, A., Maslov, O., My, T.T.T., 2006. Experimental study and theoretical consideration of the isomeric ratio in the photonuclear reaction ^{197}Au (γ, n) ^{196m,g}Au in the giant dipole resonance region. Phys. Part. Nuclei Lett. 3, 223–228. http://dx.doi.org/10.1134/S1547477106040017.

Turturica, G., Matei, C., Pappalardo, A., Balabanski, D., Chesnevskaya, S., Iancu, V., Ur, C., Karwowski, H., Chipps, K.A., Febbraro, M.T., et al., 2019. Investigation of compton scattering for gamma beam intensity measurements and perspectives at eli-np. Nucl. Instrum. Methods Phys. Res. A 921, 27–32. http://dx.doi.org/10.1016/j.nima.2018.12.048.

Veyssiere, A., Beil, H., Bergere, R., Carlos, P., Lepretre, A., 1970. Photoneutron cross sections of ^{208}Pb and ^{197}Au. Nuclear Phys. A 159 (2), 561–576. http://dx.doi.org/10.1016/0375-9474(70)90727-X.

Vlachoudis, V., 2009. Flair: A powerful but user friendly graphical interface for FLUKA. In: International Conference on Mathematics, Computational Methods & Reactor Physics 2009. pp. 790–800.

Vörös, S., Anton, M., Boillat, B., 2012. Relative response of alanine dosemeters for high-energy electrons determined using a fricke primary standard. Phys. Med. Biol. 57 (5), 1413–1432. http://dx.doi.org/10.1088/0031-9155/57/5/1413.

Xiaolong, H., 2007. Nuclear data sheets for A=196. Nucl. Data Sheets 108 (6), 1093–1286. http://dx.doi.org/10.1016/j.nds.2007.05.001.

Zilges, A., Balabanski, D., Isaak, J., Pietralla, N., 2022. Photonuclear reactions—from basic research to applications. Prog. Part. Nucl. Phys. 122, 103903. http://dx.doi.org/10.1016/j.ppnp.2021.103903.